DOI: 10.24874/ti.2056.10.25.01

Tribology in Industry

www.tribology.rs

RESEARCH

On the Probability of Melting on Sliding Surface of AISI 1020 Steel in Dry Sliding Against Quenched AISI 1045 Steel Under Electric Current

Marina Ivanovna Aleutdinova[a,*], Viktor Veniaminovich Fadin[a]

[a]*Institute of Strength Physics and Materials Science of SB RAS,Tomsk, Russia.*

Keywords:

Wear
Sliding electric contact
Transfer layer structure
Viscous melt
Friction coefficient

* Corresponding author:

Marina Ivanovna Aleutdinova
E-mail: aleut@ispms.ru

Received: 30 October 2025
Revised: 9 December 2025
Accepted: 27 January 2026

A B S T R A C T

The phase and elemental compositions of the contact layer of AISI 1020 steel (pin) were determined in dry sliding against AISI 1045 steel (disc) under mild (normal) and catastrophic wear conditions. Formation of a tribolayer on the sample contact surface was demonstrated. The layer was consisted of FeO, α-Fe, and γ-Fe phases. A study of the sample morphological features of the sliding surface revealed that this layer was deteriorated by an abrasive mechanism in one sector (sector 1) of the nominal contact area. The other sector (sector 2) was deteriorated with visual signs of melting and adhesive interaction. The main attention was paid to the oxygen concentration as an indicator of FeO formation. A high oxygen concentration (30–40 at%) was observed on the sliding surface in sector 2. Sliding surface area with melt signs was consisted of iron and oxygen. Melt signs were explained by supposition the appearance of strong pulses of electric induction vector in the contact layer (FeO-rich medium) which can transfer the FeO crystal lattice to melt state in thin contact layer during friction. The FeO-melt was not capable for strengthening the tribolayer. The oxygen concentration in the bulk of the tribolayer was less than 5 at%. This indicated weak strengthening of the contact layer due to the formation of crystalline FeO.

1. INTRODUCTION

It is known [1] that high wear resistance is achieved in the case of elastic deformation of the contact layers. This physical principle in severe conditions (oxygen-free environment, increased loads, etc.) can be fulfilled by hardening the contact layers using an appropriate method, for example, by applying wear resistant coatings [2-4]. However, plastic deformation in sliding is still inevitable on the microasperities. Even if surfaces were hardened excess hardening may cause brittleness and wear fracture. Therefore, hardening the contact surfaces by applying too hard coatings should not be used for severe friction conditions. Instead, materials capable of absorbing high contact loads and stresses may be used.

Passing high-density electric current (>100 A/cm^2) in an unlubricated sliding contact may be classified as severe sliding conditions, which definitely cause structural, phase and chemical changes in the contact layers, in particular, one of the main factor would be tribooxidation of heavily deformed and refined subsurface material. Tribooxidation would have great effect on sliding and wear as well as contact electric conductivity. For instance, sliding against a copper counterpart does not cause the formation of a large amount of oxides in the friction zone at usual temperatures lower than 100 ^{o}C. This is one of the reasons for the strong adhesion during dry sliding against copper under current. Therefore, dry sliding against copper are not used at current densities higher than 60 A/cm^2 and specific surface electrical conductivity of the contact lower than 75 S/cm^2 because of severe wear by adhesion [5]. Satisfactory wear resistance with higher electrical conductivity of the contact under high current density is achieved during dry sliding against a steel counterbody [6]. In general, the assessment of the suitability of a friction pair for sliding under current should be based on three main contact characteristics, namely, contact current density, contact electrical conductivity, and wear intensity at the end of the mild wear regime, i.e., at transition to the catastrophic wear regime.

It should be noted that the onset of catastrophic wear depends on many input parameters of the tribosystem, primarily the contact pressure, the initial structure of the contact materials and the composition of the environment. Experimental parameters such as contact configuration, turn ratio of the supply transformer, contact surface overlap coefficient, etc. can also significantly influence the onset of catastrophic wear and the three contact criterion characteristics mentioned above. A certain set of the presented tribosystem input parameters will lead to the formation of an appropriate structure of contact layers, the mechanical strength of which will determine the wear rate. It should be noted that low wear rate is the main criterion in assessing the applicability of any friction pair under any conditions. An ideal friction pair should exhibit minimal wear intensity, maximal contact electrical conductivity and maximal current density at the end of the mild wear regime. Obviously, some initial understanding of the contact interaction can be obtained by determining the wear intensity and the corresponding structure of the contact layers during sliding under current. These output parameters of the tribosystem depend primarily on the contact current density. Therefore, determining the current density range corresponding to mild wear conditions is of scientific interest. The phase and chemical compositions of the contact layers under these conditions must also be determined. This initial information can be most conveniently obtained by using simple materials and known contact configurations, for example, a pin-on-disc contact of steel/steel pair similar to those used previously [7]. Under these conditions the pin sample experiences higher wear compared to that of the counterpart-disc. Therefore, we may focus on analyzing structural, phase and tribochemical changes in a steel pin only.

The aim of this study is to obtain an initial information on the relationship between the structure of the steel contact layer and contact characteristics of steel/steel pair under mild and catastrophic wear conditions in dry sliding under electric current.

2. EXPERIMENTAL DETAILS

2.1 Materials characterization

The commercial AISI 1020 steel (0.14÷0.22 %C, 0.3÷0.6 %Mn, (S, Si, P, Cr < 0.3 %), Fe - balance) was used to fabricate the sample pins with the dimensions of 2.5 mm×4 mm in the nominal contact area and a length of 10 mm. The 1020 steel was hardened by deformation to the microhardness value of H_μ=2.4 GPa The commercial AISI 1045 steel (0.42÷0.50 %C, 0.6÷0.9 %Mn, (S, Si, P, Cr < 0.3 %), Fe - balance) was quenched to a microhardness value of H_μ=5.8 GPa (53 HRC) and used as the counterbody (disc). The Vickers microhardness (H_μ) of these steels was determined by a TVM-5215-A hardness tester under the load of about 1 N. The micrographs of the contact layer cross-sections, worn surfaces and their EDX chemical compositions were obtained using Quanta 200 3D scanning electron microscope (SEM). The X-ray diffraction (XRD) pattern of worn surface was recorded with a DRON-7 X-ray diffractometer in CoK_α radiation.

2.2 Tribological measurements

The samples were tested in dry sliding under the alternating current collection (50 Hz) at a contact pressure of p=0.13 MPa, a sliding velocity of v=5 m/s applying a well-known *pin-on-disc* wear loading configuration (Fig. 1a) at a turn ratio of the supply transformer of $k=n_1/n_2$=13.

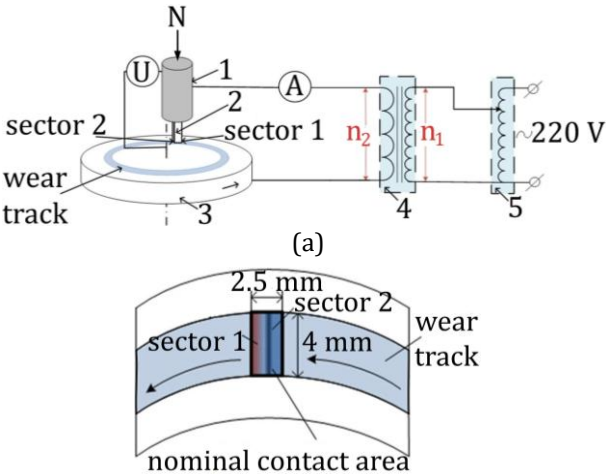

Fig. 1. (a) Schematic of a sliding electrical contact of "pin-on-disc" configuration, where 1 is the sample holder, 2 is the sample (AISI 1020 steel), 3 is the counterbody (AISI 1045 steel), 4 is the supply transformer, 5 is the autotransformer ; (b) fragment of contact scheme in the vicinity of nominal contact area (top view).

The linear wear intensity was determined as $I_h=h/D$, where h is the sample height variation per sliding distance D. The contact current density j was found as $j=i_c/A_a$, where i_c is the contact current (in the secondary winding circuit of the transformer) and A_a is the nominal surface of the tribocontact. The contact current density had some value for each sliding distance D≥9 km. The specific contact surface conductivity was obtained as $\sigma_A=j/U$ (U is the contact voltage drop). The friction coefficient μ values were found using tension-sensor (gauge) and simultaneously recorded and saved as data-files. Each test was repeated 3 times for obtaining reproducible results.

3. RESULTS

Increasing the contact current density to j=110 A/cm² does not cause a noticeable increase in the wear intensity I_h. Then I_h increases at j>110 A/cm² (Fig. 2a) and a sharp increase in I_h is observed at j≈140 A/cm². This indicates the onset of catastrophic wear. The $\sigma_A(j)$ dependence is a curve with a maximum at j=140 A/cm², where the maximum corresponds to a sharp increase in I_h (Fig. 2a). At the same time, the slope of the contact voltage drop $U(j)$ dependence increases (Fig. 2b).

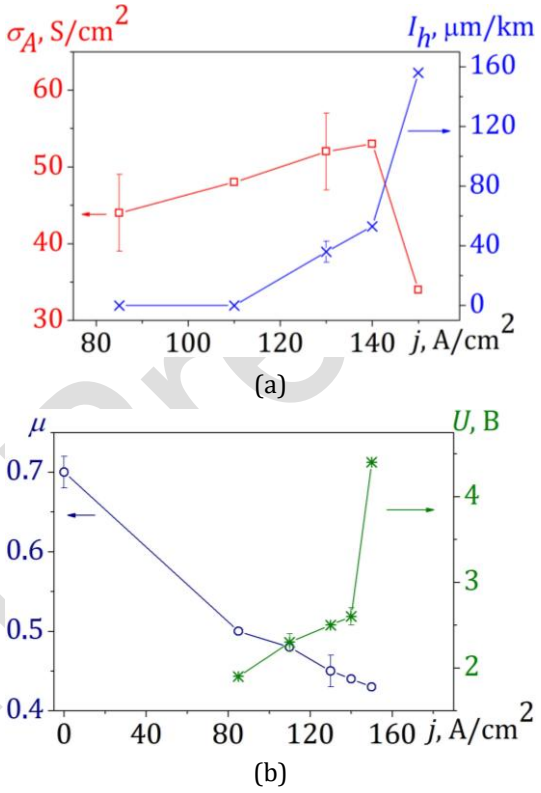

Fig. 2. Dependencies: (a) of wear intensity (I_h) of steel and contact electrical conductivity (σ_A) and (b) of friction coefficients (μ) and of voltage drop (U) on current density in 1020 steel/1045 steel contact.

It is also evident here that the friction coefficient μ decreases with increasing j and does not change its behavior at the onset of catastrophic wear. It can be seen that the mild wear mode of a sliding steel/steel electrical contact can occur at j≤140 A/cm² under laboratory conditions.

The morphological features of the sliding surface allow us to observe two sectors (Fig. 3a), which arose via two different deterioration mechanisms under mild wear conditions. The surface sector (sector 1) located on the leading part of the pin (Fig. 1), is deteriorated predominantly via plowing of the sample contact layer by harder asperities of the counterbody. The known mechanisms of plastic material deterioration by adhesive wear, delamination due to fatigue, plowing, etc. are realized in this sector which are described, for example, elsewhere [1,3,6].

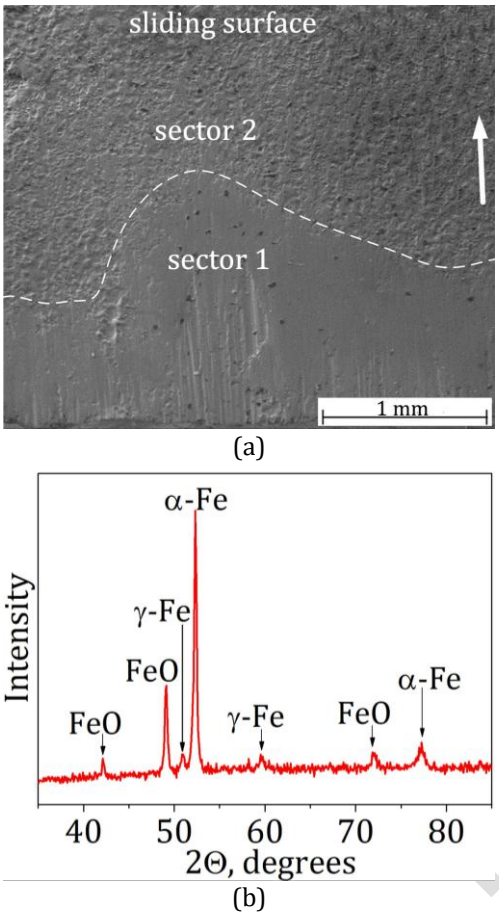

Fig. 3. (a) SEM images of the worn surface of the 1020 steel in the nominal area and (b) XRD pattern of the nominal worn surface in sliding at j=130 A/cm^2 (mild wear regime). The arrow shows the counterbody sliding direction.

The rear part of the pin's surface shows wear traces (sector 2, Fig. 1) similar to those of quasi-viscous flow (upper part of Fig. 3). Here clear traces of adhesion wear, delamination and other signs of known types of the sliding surface deterioration are absent. No glow of the sliding surface and the contact zone is observed during sliding at these conditions. This means that the average temperature on the sliding surface is below 600°C.

The noted morphological division of the sliding surface into two sectors has been observed previously [6,7], but the chemical composition has not been determined This morphological difference (Fig. 3a) between the worn surfaces of sector 1 and sector 2 allows for suggesting structural or chemical differences between these sectors. Therefore, determining the chemical composition on the full nominal contact area does not make sense and it is reasonable to find elemental compositions of sector 1 and sector 2.

The XRD pattern of the worn nominal surface of 1020 steel contains α-Fe, γ-Fe, and FeO peaks (Fig. 3b). Obviously, FeO and γ-Fe were formed under impact of friction and current, indicating that the contact layer has a composite structure. The lattice parameters of the α-Fe, γ-Fe, and FeO phases are close to their standard values from ASTM Standard database.

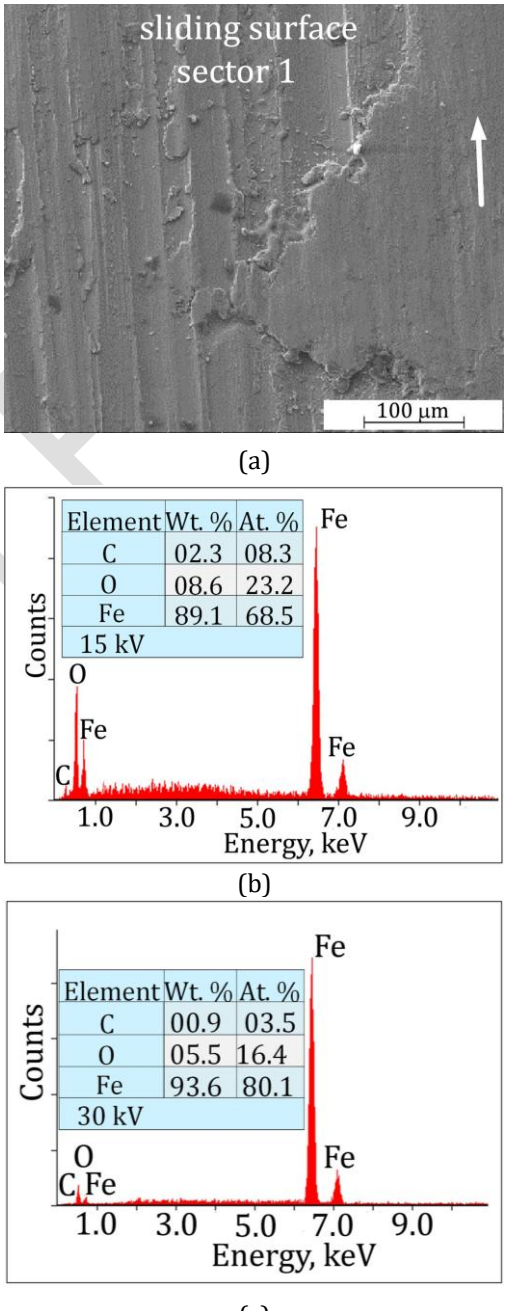

Fig. 4. (a) SEM images of the worn surface in the sector 1 of the 1020 steel in the nominal area and corresponding EDX data at accelerating voltages of (b) 15 kV and c) of 30 kV (j=130 A/cm^2, mild wear regime). The arrow shows the counterbody sliding direction.

Morphological details of the sliding surface in sector 1 reveal signs of adhesion, plowing, abrasive wear and smearing of deformed fragments of the third body onto the contact surface (Fig. 4a). Here, plastic deformation by shear and normal loads results in an average chemical composition based on carbon, oxygen, and iron (Fig. 4b, c). The main attention should be paid to the oxygen concentration as an indicator of FeO formation. The FeO content can be approximately determined by multiplying the atomic oxygen concentration by two. The distribution of iron oxide below the worn surface may be approximately derived using a dependence of electron beam penetration into a substance on the SEM accelerating voltage. It is well-known that decrease in the accelerating voltage in the electron microscope leads to decrease in the depth of electron penetration into contact layer. Therefore, high oxygen concentration near the sliding surface may be shown only by using of low accelerating voltage in the electron microscope. Relatively high value of oxygen concentration near the sliding surface compairing with that in the contact layer depth (Fig. 4b, c) is caused by more intensive iron oxidation near the sliding surface, but does not mean the formation of a FeO concentration gradient. The high carbon concentration was obtained at 15 kV (Fig. 4b, c), i.e. the carbon concentration on the surface is higher than that below the worn surface.

The absence of signs of adhesion, delamination, plastic deformation and the presence of signs of clear melting and a large number of small cracks in different directions, are the defining morphological features of the sliding surface in sector 2 (Fig. 5a). Carbon, oxygen, and iron are the main chemical elements here (Fig. 5b, c).

One can see (Fig. 6) that this composite contact layer adheres quite satisfactorily to the base metal of the 1020 steel. However, this is not always observed, as shown elsewhere [6]. Cracks perpendicular to the sliding direction and formed due to friction fatigue or thermal stresses are sometimes observed. Other discontinuities (pores, horizontal cracks, etc.) are rarely observed. The tribolayer consists of iron, oxygen, and carbon (Table 1). It should be noted that the same chemical elements are inherent in any fragment of the tribolayer (see Fig. 4 and Fig. 5) judging by the almost similar EDX spectra. Therefore, it seems reasonable to provide tables with compositions rather than spectra or maps of elements, since the tables contain all basic information. It can be seen (Table 1) that the oxygen concentration changes insignificantly with the depth of the tribolayer (area 1 and area 2, Fig. 6). In addition, the oxygen concentration is low compared to that on the sliding surface (Fig. 4 and Fig. 5). This indicates that the main quantity of FeO is formed mainly within the very thin contact layer adjacent to the sliding surface.

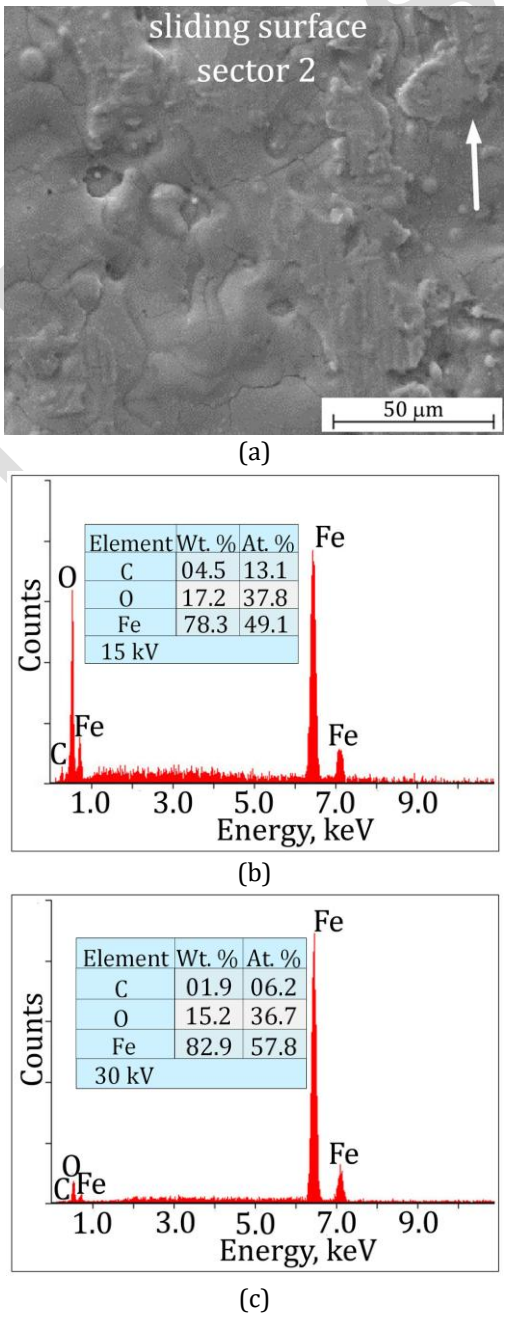

Fig. 5. Worn surface in the sector 2 (SEM image) (a) and corresponding EDX data at accelerating voltages of 15 kV (b) and of 30 kV (c) (j=130 A/cm^2, mild wear regime). The arrow shows the counterbody sliding direction.

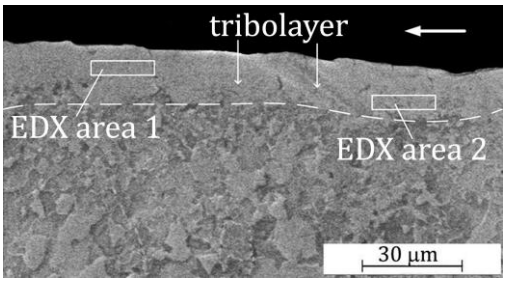

Fig. 6. SEM image of tribolayer cross-section in the section in the sector 2 (j=130 A/cm^2, mild wear regime). The arrow shows the counterbody sliding direction.

Table 1. Distribution of chemical elements in the contact layer depth at accelerating voltage of 30 kV.

Element	Wt%	At%	Wt%	At%
C K	2.2	9.3	2.4	10.1
O K	1.2	3.7	1.3	4.2
Fe K	96.6	87.0	96.2	85.7
	Area 1		Area 2	

It is of interest to compare the data corresponding to the mild wear mode with similar data corresponding to catastrophic wear. It is evident (Fig. 7) that the worn surface is morphologically divided into two sectors. These sectors have features close to those presented above and visually differ little from the images of the two sectors (Fig. 4 and Fig. 5) corresponding to mild wear. The oxygen concentration in the sector 1 decreases with the increase in accelerating voltage (Table 2). This indicates that the FeO concentration on the sliding surface is higher than that in the depth of the tribolayer. Here, the oxygen concentration values in sector 1 are higher than that in the sector 1 corresponding to mild wear (Fig. 4b, c). It is also evident that the catastrophic wear mode causes the appearance of a small amount of Mn and Cr in the tribolayer (Table 2).

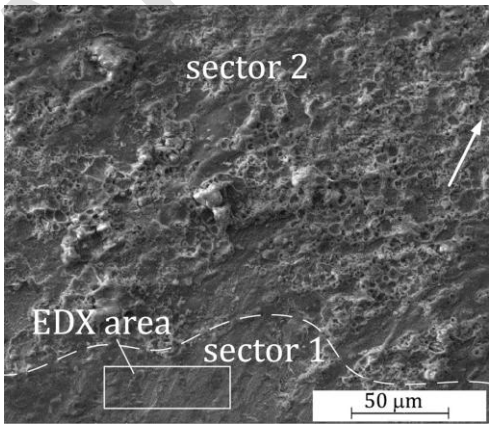

Fig. 7. SEM image of 1020 steel worn surface in the nominal area (j=150 A/cm^2, catastrophic wear). The arrow shows the counterbody sliding direction.

Table 2. Distribution of chemical elements on the worn surface in the sector 1 at accelerating voltages of 10÷30 kV (j=150 A/cm^2, catastrophic wear).

Element	At.%	At.%	At.%
C	21.3	24.5	18.5
O	39.3	32.6	29.2
Cr	2.2	1.5	2.0
Mn	1.1	0.6	0.3
Fe	36.1	40.8	50.0
Accelerating voltage	10 kV	20 kV	30 kV

Sector 2 visually contains signs of melt and solid-phase agglomerate placed in the solidified melt, where the agglomerates form crusts over large areas (Fig. 8) with cracks of varying sizes.

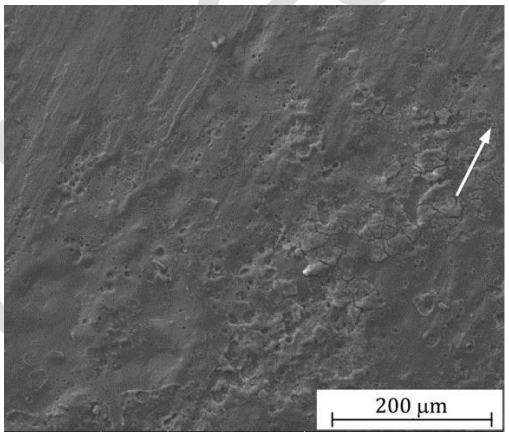

Fig. 8. SEM image of the sliding worn surface in the sector 2 (j=150 A/cm^2, catastrophic wear regime). The arrow shows the counterbody sliding direction.

Regions with a small number of agglomerates in the melt are free of cracks. Traces of electrical discharges are also visible here. There are no obvious signs of severe plastic deformation of the contact layer. The average oxygen concentration increases according to decrease in accelerating voltage in the microscope (Table 3). This indicates relatively intensive FeO formation near the sliding surface. The FeO concentration in sector 2 is slightly higher than that in sector 2 corresponding to normal wear (Fig. 5b.c). Small amounts of Mn and Cr were also detected.

It was shown above (Fig. 3b) that FeO is the only high-modulus phase in the tribolayer and the solid phase agglomerates should be FeO-based. It is evident (Fig. 9) that the agglomerate has a large number of cracks and traces of electrical discharges. Cracks are due to the high oxygen content (Table 4), i.e., to high FeO concentration,

strong mechanical stress pulses, or thermal stresses appeared as a result of fast cooling. It is possible that catastrophic wear is conditioned owing to separating of large microvolumes (Fig. 9). It is possible that Cr and, especially, Mn (Table 4) cause locally some increase in the electrical resistance of the contact layer. This can create high temperature gradients in the contact zone and provide an additional contribution to the deterioration of the contact layer.

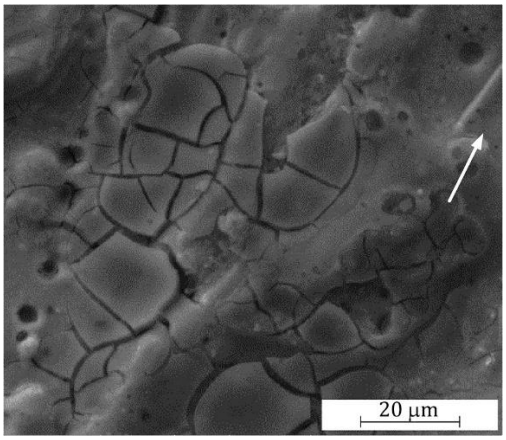

Fig. 9. SEM image of the agglomerate fragment in the sector 2. The arrow shows the counterbody sliding direction.

Table 3. Distribution of chemical elements on the worn surface in the sector 2 at accelerating voltages of 10, 20, and 30 kV (j=150 A/cm^2, catastrophic wear regime).

Element	At.%	At.%	At.%
C	11.4	14.3	21.9
O	43.7	39.6	34.4
Cr	2.6	1.9	1.5
Mn	1.5	0.6	0.5
Fe	40.8	43.6	41.7
Accelerating voltage	10 kV	20 kV	30 kV

Table 4. Chemical element concentrations in sector 2 at accelerating voltages of 10, 20, and 30 kV (j = 150 A/cm^2, catastrophic wear regime).

Element	At.%	At.%	At.%
C	10.6	12.4	3.1
O	42.1	39.5	42.2
Cr	2.1	2.0	2.4
Mn	1.8	0.9	0.9
Fe	43.4	45.2	51.4
Accelerating voltage	10 kV	20 kV	30 kV

The tribolayer thickness (Fig. 10) and the average concentrations of its main elements (Table 5) under catastrophic wear conditions are close to those under mild wear conditions (Fig. 6). It can be concluded that the parameters of the tribolayer cross-section, i.e., its base do not change significantly upon transition to catastrophic wear. One can see that the concentration gradient of oxygen (and FeO) is not clearly observed.

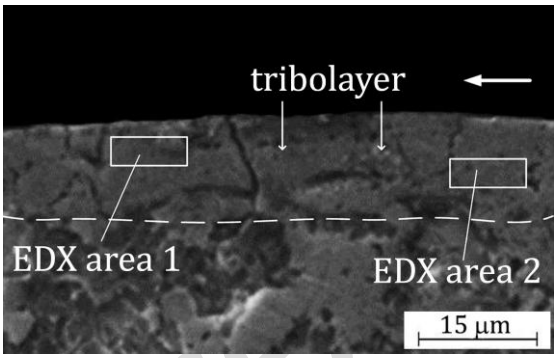

Fig. 10. SEM image of sliding surface cross-section in the sector 2 (j = 150 A/cm^2, catastrophic wear regime). The arrow shows the counterbody sliding direction.

Table 5. Distribution of chemical elements across the transfer layer depth from Fig. 10 at accelerating voltage of 30 kV (j = 150 A/cm^2, catastrophic wear).

Element	Wt%	At%	Wt%	At%
C K	2.2	9.4	2.5	10.3
O K	1.0	3.0	1.3	3.9
Fe K	96.8	87.6	96.2	85.8
	Area 1		Area 2	

4. DISCUSSION

Oxygen can mainly exist in FeO crystals after friction. Therefore, the oxygen concentration (above 30 at.%) in sector 2 indicates that more than half of the contact layer atoms belong to FeO. This means that the main volume of the melt consists of oxygen and iron ions. As was shown above (Fig. 3b), FeO is the only oxide on the sliding surface. This means that only FeO melts during friction under current and sliding. Here an increase in the concentration of carbon and oxygen at approaching to sliding surface is shown by a decrease in accelerating voltage in the microscope. A small difference in oxygen concentration with a change in accelerating voltage in the microscope indicates the formation of a quite thick layer containing FeO (Fig. 5b,c and Fig. 9). Definition of this layer thickness is not the object of this work. The oxygen concentration, as an indicator of FeO formation, is significantly higher in sector 2 than in sector 1. The iron

concentration is always higher than the oxygen concentration that indicates the formation of composite of composition of FeO+(α-Fe)+(γ-Fe) in the contact layer.

Manganese and chromium can appear in the contact layer from the original structure through various mechanisms. Currently, it can only be noted that they appeared under conditions of catastrophic wear, and this information cannot yet be satisfactorily applied. Carbon can be present in Fe_3C, in γ-Fe, or in free form deep within the tribolayer. However, its state during friction is unknown. In general, low concentrations of carbon, manganese, and chromium do not allow for a definitive determination of their influence on friction behavior. Therefore, a detailed discussion of their presence cannot be satisfactorily substantiated and is not included in this paper.

The mechanism for the formation of the melt and two sectors on the sliding surface was proposed elsewhere [8], where Hadfield steel was subjected to sliding under electric current. It is shown above that contact layer is a medium containing ionic insulator (FeO), i.e, it is an environment capable of polarizing. Sliding in stick-slip mode is realized always without lubricants. The stage "slip" should cause weak electric contact, which must be compensated by self-induction current pulse. One may suppose that such pulse can induce electrical induction vector pulse which may be capable provide FeO ions with sufficient energy to escape the crystal lattice nodes and form a melt in the FeO-rich regions of the contact layer. It should be noted that this is only one of the explanations, i.e. the assumption should be checked, since the current of free charges can prevail over the current of connected charges. If an increase in contact current density causes an increase in the melt volume, i.e. an increase in the number of charge carriers (Fe^{2+} and O^{2-} ions), the contact electrical conductivity increases (Fig. 2a). The increase in melt volume leads to more free moving of the sample contact surface relatively to that of the counterbody. In general, melt formation is one of the ways to dissipate the energy of external impact. The reduction in the coefficient of friction during sliding in a lubricant (in the absence of the stick-slip mode) or without current occurs without the appearance of electric induction vector pulses and melting is not observed [8-12].

The formation of two sectors occurs due to the obvious difference in the contact interaction of the counterbody with the advancing and opposite edges of the sample nominal contact area [8]. It is known [6] that the tribolayer contains more than 70 vol.% FeO on the contact surface of the counterbody. The advancing edge (directed towards the movement of the counterbody contact surface) comes into contact with this FeO-rich tribolayer and brittle deterioration of the tribolayers of the sample and the counterbody occurs. In this case, the advancing edge of the sample is deformed by brittle FeO-rich fragments and the contact surface of the sample takes the form shown in Fig. 4a (sector 1). FeO-rich fragments move from sector 1 to sector 2, oxidize and simultaneously melt under impact of electric induction vector pulses. Obviously, these fragments have the maximum FeO content and maximum signs of melting (sector 2, Fig. 5a) upon exiting sector 2 onto the surface of the counterbody [8]. However, the morphological features of sector 2 cannot show signs of plastic deformation because the sliding surface is coated with melt. It follows from here, that crystalline FeO does not exist on the sliding surface during friction and therefore, cannot strengthen it or reduce wear. But FeO can exist in the tribolayer depth.

Usually the tribolayer is formed, particularly, due to the rotational mode of plastic deformation. It can be assumed that solid FeO forming on the sliding surface moves to the layer depth due to rotation. Then the cross section of the tribolayer will contain a fairly high concentration of crystalline FeO, distributed uniformly. However, this is not observed (Table 1 and Table 4). Such a low FeO content in the depth of the tribolayer can be explained by the fact that the FeO melt is weakly displaced by rotation into the internal volumes of the trbolayer and remains mainly on the sliding surface. It can be assumed that the tribolayer consists of a thin FeO-rich composite layer of the composition of FeO + α-Fe + γ-Fe + C (>60 vol.% FeO) as a melt adjacent to the (contact) sliding surface and a thicker FeO-poor layer of the composition FeO + α-Fe + γ-Fe + C (<20 vol.% FeO) during friction, where FeO is in the crystalline state. This FeO-poor layer serves as the base of the entire tribolayer where FeO exists in a crystalline state and can strengthen the tribolayer. The high FeO concentration in the thin layer of solidified melt near the sliding surface causes brittle fracture during the production of

grind or foil. Therefore, the use of some materials science methods (e.g., EBSD or TEM) may not be successful (i.e. without satisfactory results).

It should be assumed that a thin melt sublayer does not provide completely liquid friction between the contact surfaces since the friction coefficient has a value close to that of dry metal/metal friction. This indicates a mechanical and adhesive interaction of counterbody contact surface asperities with the sample FeO-poor sublayer. In general, alloying elements or particles of solid phases should cause a decrease in the ductility of this layer, i.e., reduce its ability to relax stresses under conditions of inevitable plastic deformation of the contact layer. Then the formation of microcracks and fracture fragments is the most probable way of stress relaxation in the layer. Therefore, tribolayer containing alloying elements or particles of solid phases (carbides, oxides, etc.) usually fail quite intensively under variable loads exceeding their yield strength [2,13-16]. It was noted above, that strengthening the contact layer by alloying or oxides can be useful only for loads causing elastic deformation. The FeO-poor tribo-sublayer (Fig. 6 and Fig. 10) of the (FeO+α-Fe+γ-Fe+C) composition indicates a fairly high concentration of the ductile α-Fe and γ-Fe phases, which are the matrix of this composite sublayer. Therefore, wear resistance, being an indicator of the strength of this layer, is conditioned mainly by the ductility of these phases. Satisfactory thermal conductivity of these iron phases provides an additional contribution to wear resistance.

Sometimes the contact characteristics are improved due to the presence of a gradient structure [17-20]. Different oxygen concentrations into different tribolayer depths shown by different accelerating voltages in a microscope suggest the presence of FeO concentration gradients. However, this assumption requires additional confirmation. The metallographic structure of the tribolayer does not contain clear signs of a FeO concentration gradient (Fig. 6 and Fig. 10). The absence of a gradient structure was also shown in [8]. Therefore, it seems reasonable to conceptualize the tribolayer structure as a system of two sublayers, where a thin FeO-rich melt sublayer is adjacent to the sliding surface and a thick FeO-poor sublayer is adjacent to the original structure of 1020 steel during sliding. This concept of the tribolayer was proposed above in the analysis of the data on the tribolayer structure in sector 2. Here, a similar structure should be formed in sector 1, where the thickness of the FeO-rich melt sublayer approaches zero and only traces of abrasive wear are visible. The thickness of the FeO-rich melt sublayer should increase as the observation point moves closer to sector 2, and this thickness reaches a maximum when the melt exits in sector 2 onto the sliding surface of the counterbody. But there are difficulties to observe this effect.

5. CONCLUSION

Dry sliding of AISI 1020 steel against AISI 1045 steel in a pin-on-disc configuration under alternating electric current was carried out to study the failure character of 1020 steel contact surface and to determine the oxygen distribution as an indicator of FeO formation. The following findings were obtained:

1. A composite tribolayer approximately of 10 μm thick was observed on the 1020 steel contact surface. The layer had a phase composition of FeO + α-Fe + γ-Fe + C.
2. Changes in the tribosystem during friction were represented by the formation of two morphologically different sectors on the contact surface. One of the sectors (Sector 1) showed traces of abrasive interaction, while the other sector (sector 2) showed signs of melting.
3. Sector 1 contained less than 25 at.% oxygen. Sector 2 contained more than 30 at.% oxygen, indicating the presence of more than 60 vol.% FeO after friction.
4. The tribolayer can be represented as a system of two sublayers, where a thin FeO-rich melt sublayer is adjacent to the sliding surface and a thick FeO-poor sublayer is adjacent to the original structure of 1020 steel.
5. It was noted that the system of Fe^{2+} and O^{2-} ions could exist in molten state under impact of strong self-induction pulses and corresponding pulses of electric induction vector that arose during stick-slip sliding.
6. The presented results provide a new contribution to the understanding of processes in the friction zone and will be useful for high-power low-voltage electric motors design having small sizes.

CRediT authorship contribution statement

Marina Ivanovna Aleutdinova: Writing – original draft, Methodology, Conceptualization.
Viktor Veniaminovich Fadin: Writing – review & editing, Investigation, Supervision.
Declaration of Competing Interest

The authors declare that they have no known competing financial interests or personal relationships that could have appeared to influence the work reported in this paper.

Acknowledgements

The study was carried out within a state task of the ISPMS SB RAS, project No FWRW-2026-0001.

REFERENCES

[1] I.V. Kragelsky, M.N. Dobychin and V.S. Kombalov, *Friction and Wear Calculation Methods*, New York: Pergamon Press, 1982.

[2] R. G. Zheng, Z. J. Zhan, and W. K. Wang, "Wear behavior of Cu–La2O3 composite with or without electrical current," *Wear*, vol. 268, no. 1–2, pp. 72–76, Jun. 2009, doi: 10.1016/j.wear.2009.06.026.

[3] V. K. Matsagar, U. M. Shirsat, and P. B. Kushare, "NI-CR based self lubricating composite performance for high speed engineering application," *Tribology in Industry*, vol. 46, no. 1, pp. 1–12, Mar. 2024, doi: 10.24874/ti.1469.04.23.06.

[4] V. Chitanov *et al.*, "Elastic-Plastic Properties of hard Cr-Based Nitride Coatings Deposited at Temperatures Below 200°C," *Tribology in Industry*, vol. 45, no. 1, pp. 340–350, Jun. 2023, doi: 10.24874/ti.1460.03.23.05.

[5] M. Braunovic, V. V. Konchits, and N. K. Myshkin, *Electrical Contacts: Fundamentals, Applications and Technology*, 1st ed. CRC Press, 2017, doi: 10.1201/9780849391088.

[6] M. Aleutdinova and V. Fadin, "Effect of the initial structure of steels on the deterioration of their contact layers in dry sliding against quenched steel under alternating electric current of a density higher than 100 A/cm2," *Wear*, vol. 572–573, p. 205985, Feb. 2025, doi: 10.1016/j.wear.2025.205985.

[7] M. I. Aleutdinova, A. V. Kolybaev, and V. V. Fadin, "Structure of Contact Layer of Steel (0.2% C) and Electrical Conductivity of Contact in Sliding on Steel Under Alternative Electric Current with Different Turn Ratios of Current Source," *Russian Physics Journal*, vol. 65, no. 6, pp. 1041–1047, Oct. 2022, doi: 10.1007/s11182-022-02730-1.

[8] M. Aleutdinova and V. Fadin, "On gradients of FeO concentration in the contact layer of Hadfield steel in dry sliding against C45 steel under electric current," *Wear*, vol. 582–583, p. 206361, Sep. 2025, doi: 10.1016/j.wear.2025.206361.

[9] S. Q. Wang, M. X. Wei, and Y. T. Zhao, "Effects of the tribo-oxide and matrix on dry sliding wear characteristics and mechanisms of a cast steel," *Wear*, vol. 269, no. 5–6, pp. 424–434, May 2010, doi: 10.1016/j.wear.2010.04.028.

[10] H. Kato, "Effects of supply of fine oxide particles onto rubbing steel surfaces on severe–mild wear transition and oxide film formation," *Tribology International*, vol. 41, no. 8, pp. 735–742, Mar. 2008, doi: 10.1016/j.triboint.2008.01.001.

[11] N. Argibay, J. A. Bares, J. H. Keith, G. R. Bourne, and W. G. Sawyer, "Copper–beryllium metal fiber brushes in high current density sliding electrical contacts," *Wear*, vol. 268, no. 11–12, pp. 1230–1236, Feb. 2010, doi: 10.1016/j.wear.2010.01.014.

[12] Y. Yang, A. Meng, X. Chen, and Y. Zhao, "Tribo-induced surface deformation mechanisms govern friction and wear in ultra-light HCP and duplex Mg–Li alloys," *Wear*, vol. 510–511, p. 204507, Sep. 2022, doi: 10.1016/j.wear.2022.204507.

[13] M. Demirel, M. Muratoglu, "The friction and wear behavior of Cu-Ni_3Al composites by dry sliding," *Materials and technology*, vol. 45, no.5, pp. 401-406, Jan. 2011.

[14] S. G. Jia, P. Liu, F. Z. Ren, B. H. Tian, Zheng, and G. S. Zhou, "Sliding wear behavior of copper alloy contact wire against copper-based strip for high-speed electrified railways," *Wear*, vol. 262, no. 7–8, pp. 772–777, Oct. 2006, doi: 10.1016/j.wear.2006.08.020.

[15] L. Zhang, X. Luo, J. Liu, Y. Leng, and L. An, "Dry sliding wear behavior of Mg-SiC nanocomposites with high volume fractions of reinforcement," *Materials Letters*, vol. 228, pp. 112–115, May 2018, doi: 10.1016/j.matlet.2018.05.114.

[16] F. E. Kennedy, Y. Lu, I. Baker, and P. R. Munroe, "The influence of sliding velocity and third bodies on the dry sliding wear of Fe30Ni20Mn25Al25 against AISI 347 stainless steel," *Wear*, vol. 374–375, pp. 63–76, Jan. 2017, doi: 10.1016/j.wear.2017.01.002.

[17] P. F. Wang, Z. Han, and K. Lu, "Enhanced tribological performance of a gradient nanostructured interstitial-free steel," *Wear*, vol. 402–403, pp. 100–108, Feb. 2018, doi: 10.1016/j.wear.2018.02.010.

[18] W. Kong, D. Zhang, Q. Tao, K. Chen, J. Wang, and S. Wang, "Wear properties of the deep gradient wear-resistant layer applied to 20CrMnTi gear steel," *Wear*, vol. 424–425, pp. 216–222, Feb. 2019, doi: 10.1016/j.wear.2019.02.026.

[19] K. Zhang and Z. B. Wang, "Strain-induced formation of a gradient nanostructured surface layer on an ultrahigh strength bearing steel," *Journal of Material Science and Technology*, vol. 34, no. 9, pp. 1676–1684, Dec. 2017, doi: 10.1016/j.jmst.2017.12.012.

[20] Q. Guo *et al.*, "Dual-gradient structure enhances wear resistance of aero-engine bearing steel by suppressing strain localization," *Acta Materialia*, vol. 289, p. 120919, Mar. 2025, doi: 10.1016/j.actamat.2025.120919.